Nat. Hazards Earth Syst. Sci. Discuss., 2, 2151–2183, 2014
www.nat-hazards-earth-syst-sci-discuss.net/2/2151/2014/
doi:10.5194/nhessd-2-2151-2014

Natural Hazards and Earth System Sciences
Discussions
Open Access

A two-phase model for numerical simulation of debris flows

S. He[1,2], W. Liu[2], C. Ouyang[1,2], and X. Li[1,2]

[1]Key laboratory of Mountain Hazards and Earth Surface process, Chinese Academy of Science, Chengdu, China
[2]Institute of Mountain Hazards and Environment (IMHE), Chinese Academy of Sciences, Chengdu, China

Received: 21 January 2014 – Accepted: 23 February 2014 – Published: 25 March 2014

Correspondence to: X. Li (lixinpo@imde.ac.cn)

Published by Copernicus Publications on behalf of the European Geosciences Union.

Abstract

Debris flows are multiphase, gravity-driven flows consisting of randomly dispersed interacting phases. The interaction between the solid phase and liquid phase plays a significant role on debris flow motion. This paper presents a new two-phase debris flow model based on the shallow water assumption and depth-average integration. The model employs the Mohr–Coulomb plasticity for the solid stress, and the fluid stress is modeled as a Newtonian viscous stress. The interfacial momentum transfer includes viscous drag, buoyancy and interaction force between solid phase and fluid phase. We solve numerically the one-dimensional model equations by a high-resolution finite volume scheme based on a Roe-type Riemann solver. The model and the numerical method are validated by using one-dimensional dam-break problem. The influences of volume fraction on the motion of debris flow are discussed and comparison between the present model and Pitman's model is presented. Results of numerical experiments demonstrate that viscous stress of fluid phase has significant effect in the process of movement of debris flow and volume fraction of solid phase significantly affects the debris flow dynamics.

1 Introduction

Debris flows, which are mixtures by solid sediments and saturated water, are one of extremely destructive natural hazards to human lives due to its high speed and huge impulsive forces (Iverson, 2012; McDougall and Hungr, 2005; Richenmann, 1999; Pitman et al., 2003; Medina, 2008). The debris flows are usually occurred owing to storm rainfall or snow melting and are classical two-phase, gravity-driven flows consisting of a broad distribution of grain sizes mixed with fluid. The flow behavior greatly depends on both the sediment composition and the volume fraction of solid phase. A debris-flow model which can efficiently depict the stress of solid sediment, the fluid phase and the interaction forces across their interfaces, is essential to properly predict its run-out distance and hazardous areas.

Following the pioneering work of Savage and Hutter (1989), in the past few decades, great achievements have been made in the numerical simulating of debris flows by means of depth-integrated theory. In Savage–Hutter (S–B) model (1989), the flowing layer on one-dimensional slope is assumed to be an incompressible material and depicted by the Mohr–Coulomb behavior. Hutter et al. (1991) further suggested an improved S-H model to extend to quasi-three dimensional basal surfaces. The depth-integrated method is further applied to diverse earth-surface flows, such as dam-breaks (Carpet and Young, 1998; Cao et al., 2004; Wu and Wang, 2007; Soares-Frazão et al., 2012), debris flows (Iverson et al., 2010; Medina, 2008), floods (Denlinger and O'Connell, 2010), tsunamis (George and Leveque, 2006) and so on. Nevertheless, most of the previous models are based on single-phase assumption which considers the flows as uniform flows. However, the characteristics that the solid and fluid forces must act harmoniously in debris flows demonstrate considering the motion of two phases separately is necessary (Iverson, 1997).

The numerical simulations of debris flow based on two-phase models have been widely concerned by an increasing number of scientists. Iverson (1997) and Iverson and Denlinger (2001) considered the flow as a mixture of fluid and solid massand built. The assumed the relative velocity between the two constituents was small and thus the drag force between the solid phase and the fluid phase was neglected. However, the solid and fluid phase velocities may deviate substantially from each other in natural debris flow and the drag force has important effect on the motion of debris flow. Pitman and Le (2005) on the other hand, took the relative velocity between the solid phase and the fluid phase into account, while the fluid phase was simply assumed as ideal fluid. Pudasaini (2012) presented a new, generalized two-phase debris flow model that includes many essential physical phenomena including the effect of buoyancy, drag force and virtual mass. Mohr–Coulomb plasticity was used to close the solid stressand

NHESSD
2, 2151–2183, 2014

the fluid stress was modeled as a non-Newtonian viscous stress. But Pudasaini model is too complex and not easy to apply.

In the present work, based on the shallow water assumption and depth-average integration, a system of model equations of two-phase debris flow is constituted. The model employs the Mohr–Coulomb plasticity for the solid stress, and the fluid stress is modeled as a Newtonian viscous stress. The relative motion and interaction between the solid and fluid phases is also considered. A high-resolution finite volume scheme based on a Roe-type Riemann scheme is used to solve numerically the one-dimensional model equations of two-phase debris flow. The performance of the present two-phase and of the Pitman and Le models is comparable both in predicting debris flow evolution.

2 Equations of conservative law

We consider debris flows made of a mixture of solid and fluid materials as shown in Fig. 1. This situation can be described by Jackson's model (2000). Within the domain occupied by the mixture, the model satisfies mass conservation for the solid and fluid phases:

$$\left.\begin{aligned}&\frac{\partial(\rho_{\mathrm{s}}\varphi)}{\partial t}+\nabla\cdot(\rho_{\mathrm{s}}\varphi\nabla\boldsymbol{u}_{\mathrm{s}})=0\\&\frac{\partial\rho_{\mathrm{f}}(1-\varphi)}{\partial t}+\nabla\cdot(\rho_{\mathrm{f}}(1-\varphi)\nabla\boldsymbol{u}_{\mathrm{f}})=0\end{aligned}\right\}\tag{1}$$

and conservation of momentum for the solid and fluid phases:

$$\left.\begin{aligned}&\rho_{\mathrm{s}}\varphi\left(\frac{\partial\boldsymbol{u}_{\mathrm{s}}}{\partial t}+(\boldsymbol{u}_{\mathrm{s}}\cdot\nabla)\boldsymbol{u}_{\mathrm{s}}\right)=\rho_{\mathrm{s}}\varphi\boldsymbol{g}-\nabla\cdot\mathbf{T}_{\mathrm{s}}+\varphi\nabla\cdot p+\boldsymbol{f}\\&\rho_{\mathrm{f}}(1-\varphi)\left(\frac{\partial\boldsymbol{u}_{\mathrm{f}}}{\partial t}+(\boldsymbol{u}_{\mathrm{f}}\cdot\nabla)\boldsymbol{u}_{\mathrm{f}}\right)=\rho_{\mathrm{f}}(1-\varphi)\boldsymbol{g}-(1-\varphi)\nabla\cdot p+\nabla\cdot(1-\varphi)\boldsymbol{\tau}_{\mathrm{f}}-\boldsymbol{f}\end{aligned}\right\}\tag{2}$$

where the subscript "s" refers to the solid phase and the subscript "f" refers to the fluid phase. The velocity $\boldsymbol{u}_{\mathrm{s}}$ is for the solid phase and $\boldsymbol{u}_{\mathrm{f}}$ for the fluid phase. $\mathbf{T}_{\mathrm{s}}$ denotes the

NHESSD
2, 2151–2183, 2014

A two-phase model for numerical simulation of debris flows

S. He et al.

stress tensor of solid phase and ρ represents the density. $\boldsymbol{\tau}_\mathrm{f}$ is the extra stress for fluid. Acceleration due to gravity is denoted by $\boldsymbol{g}$. $\boldsymbol{f}$ represents the non-buoyant value of the resultant force exerted by the fluid on a solid particle. The solid volume fraction is φ. Note that both the grain density ρ_s and the fluid density ρ_f are constant, so that each material is incompressible. However, the density of the solid phase $\varphi\rho_\mathrm{s}$ and the density of the fluid phase $(1-\varphi)\rho_\mathrm{f}$ can change because φ varies with space and time.

An empirical form is proposed for the non-buoyant interaction force f (Anderson, et al., 1995; Jackson, 2000), which is the product of the relative velocity and a phenomenological constant as follows

$$f = (1-\varphi)\beta(\boldsymbol{u}_\mathrm{f} - \boldsymbol{u}_\mathrm{s}) \tag{3}$$

where the leading factor of $(1-\varphi)$ accounts for the volume of the fluid acting on the entire particle phase, β is a phenomenological function based on the experimental results of Richardson and Zaki (1954) and is expressed as

$$\beta = \frac{(\rho_\mathrm{s}-\rho_\mathrm{f})\varphi g}{V_\mathrm{T}(1-\varphi)^m} \tag{4}$$

V_T is the terminal velocity of a typical solid particle falling in the fluid under gravity, $\boldsymbol{g}$ is the magnitude of the gravitational force and m is related to the Reynolds number of the flow.

The phase-averaged viscous-fluid stresses are modeled using a Newtonian fluid rheology:

$$\tau_{ij} = -\left(p + \frac{2}{3}\mu\nabla\cdot\boldsymbol{u}\right)\delta_{ij} + 2\mu e_{ij} \tag{5}$$

here, μ is the viscous coefficient.

NHESSD
2, 2151–2183, 2014

3 Boundary conditions

Equations (1)–(4) are subject to kinematic and dynamic boundary conditions for both solid and fluid phases at the upper surface and the base. Thus, the corresponding kinematic determined by the solid phase and fluid phase at the free surface, $z_t = 0$:

$$z_t = 0: \quad \frac{\partial z_t}{\partial t} = w_s(z_t) - u_s(z_t)\frac{\partial z_t}{\partial x} - v_s(z_t)\frac{\partial z_t}{\partial y} \tag{6}$$

$$z_t = 0: \quad \frac{\partial z_t}{\partial t} = w_f(z_t) - u_f(z_t)\frac{\partial z_t}{\partial x} - v_f(z_t)\frac{\partial z_t}{\partial y} \tag{7}$$

The dynamic boundary conditions of both the solid and fluid phases are assumed to be traction free, giving

$$\mathbf{T}^f n_t = 0, \quad \mathbf{T}^s n_t = 0 \tag{8}$$

The corresponding kinematic determined by the solid phase and fluid phase at the base surface, $z_b = 0$

$$z_b = 0: \quad \frac{\partial z_b}{\partial t} = w_s(z_b) - u_s(z_b)\frac{\partial z_b}{\partial x} - v_s(z_b)\frac{\partial z_b}{\partial y} \tag{9}$$

$$z_b = 0: \quad \frac{\partial z_b}{\partial t} = w_f(z_b) - u_f(z_b)\frac{\partial z_b}{\partial x} - v_f(z_b)\frac{\partial z_b}{\partial y} \tag{10}$$

The dynamic boundary conditions of the solid phases is assumed to satisfies a Coulomb dry–friction sliding law, giving

$$z_b(\boldsymbol{x}, t) = 0, \boldsymbol{p}_b \boldsymbol{n}_b - \boldsymbol{n}_b(\boldsymbol{n}_b \cdot \boldsymbol{p}_b \boldsymbol{n}_b) = (\boldsymbol{u}_b/|\boldsymbol{u}_b|) tg\varphi(\boldsymbol{n}_b \cdot \boldsymbol{p}_b \boldsymbol{n}_b) \tag{11}$$

were the surface and basal normal are

$$\boldsymbol{n}_t = \frac{\nabla z_t}{|\nabla z_t|}, \quad \boldsymbol{n}_b = \frac{\nabla z_b}{|\nabla z_b|}$$

4 Depth-integrated equations

A key step in further simplifying the equations of motion involves depth averaging to eliminate explicit dependence on z which is the coordinate normal to the bed. The depth-averaged solid phase volume fraction, velocities and stress components are defined by $\overline{\varphi} = \frac{1}{h}\int_{z_b}^{z_t} \varphi \mathrm{d}z$, $\overline{u}_s = \frac{1}{h}\int_{z_b}^{z_t} u_s \mathrm{d}z$, $\overline{u}_f = \frac{1}{h}\int_{z_b}^{z_t} u_f \mathrm{d}z$, $\overline{v}_s = \frac{1}{h}\int_{z_b}^{z_t} v_s \mathrm{d}z$, $\overline{v}_f = \frac{1}{h}\int_{z_b}^{z_t} v_f \mathrm{d}z$, $\overline{\tau}_{ij} = \frac{1}{h}\int_{z_1}^{z_2} \tau_{ij} \mathrm{d}z$.

4.1 Depth averaged mass balance equations

We start by integrating the mass balance equation of the solid phase in the z direction. Using Leibniz' formula to interchange the differentiation and integration operators, we obtain:

$$\int_{z_b}^{z_t} \left(\frac{\partial \varphi}{\partial t} + \frac{\partial \varphi u_s}{\partial x} + \frac{\partial \varphi v_s}{\partial y} + \frac{\partial \varphi w_s}{\partial z} \right) \mathrm{d}z = \frac{\partial \overline{\varphi} h}{\partial t} + \frac{\partial \overline{\varphi} h \overline{u}_s}{\partial x} + \frac{\partial \overline{\varphi} h \overline{v}_s}{\partial y} = 0 \tag{12}$$

Assuming $\varphi(z_b) = \varphi_b$, Eq. (12) reduces to:

$$\frac{\partial \overline{\varphi} h}{\partial t} + \frac{\partial \overline{\varphi} h \overline{u}_s}{\partial x} + \frac{\partial \overline{\varphi} h \overline{v}_s}{\partial y} = 0 \tag{13}$$

Similarly, by integrating the mass balance equation of the fluid phase the z direction and using Leibniz' formula to interchange the differentiation and integration operators,

NHESSD
2, 2151–2183, 2014

we obtain:

$$\int_{z_b}^{z_t}\left(\frac{\partial(1-\varphi)}{\partial t}+\frac{\partial(1-\varphi)u_f}{\partial x}+\frac{\partial(1-\varphi)v_f}{\partial y}+\frac{\partial(1-\varphi)w_f}{\partial z}\right)\mathrm{d}z = \tag{14}$$

$$\frac{\partial(1-\overline{\varphi})h}{\partial t}+\frac{\partial(1-\overline{\varphi})h\overline{u}_f}{\partial x}+\frac{\partial(1-\overline{\varphi})h\overline{v}_f}{\partial y}=0$$

$$\frac{\partial(1-\overline{\varphi})h}{\partial t}+\frac{\partial(1-\overline{\varphi})h\overline{u}_f}{\partial x}+\frac{\partial(1-\overline{\varphi})h\overline{v}_f}{\partial y}=0 \tag{15}$$

4.2 Depth averaged momentum balance equations

4.2.1 Solid-phase

To obtain the averaged momentum balance equations for the solid phase, here only the x-direction solid momentum equation is considered. By depth-averaging the inertial part of the equation and applying the kinematic boundary conditions together with the Leibniz rule of integration.The left-hand side of the x-momentum equation of the solid phase can be written as

$$\mathrm{LHS}=\frac{\partial(\rho_s\varphi u_s)}{\partial t}+\frac{\partial\left(\rho_s\varphi u_s^2\right)}{\partial x}+\frac{\partial(\rho_s\varphi u_s v_s)}{\partial y}+\frac{\partial(\rho_s\varphi u_s w_s)}{\partial z}$$

Depth averaging and using boundary conditions yields

$$\int_{z_b}^{z_t}\mathrm{LHS}\,\mathrm{d}z=\int_{z_b}^{z_t}\left[\frac{\partial(\varphi\rho_s u_s)}{\partial t}+\frac{\partial\left(\varphi\rho_s u_s^2\right)}{\partial x}+\frac{\partial(\varphi\rho_s u_s v_s)}{\partial y}+\frac{\partial(\varphi\rho_s u_s w_s)}{\partial z}\right]\mathrm{d}z$$

$$\int_{z_b}^{z_t} \mathrm{LHS}\mathrm{d}z = \rho_s \left(\frac{\partial \left(h\overline{\varphi u_s} \right)}{\partial t} + \frac{\partial \left(h\overline{\varphi u_s^2} \right)}{\partial x} + \frac{\partial \left(h\overline{\varphi u_s v_s} \right)}{\partial y} \right) \tag{16}$$

Now, depth-averaging the right-hand side of the x-momentum equation of the solid phase yields:

$$\int_{z_b}^{z_t} (\mathrm{RHS})\mathrm{d}z = \int_{z_b}^{z_t} \left[\rho_s \varphi g_x - \frac{\partial (T_{sxx})}{\partial x} - \frac{\partial (T_{sxy})}{\partial y} - \frac{\partial (T_{sxz})}{\partial z} + p\frac{\partial \varphi}{\partial x} + (1-\varphi)\frac{(\rho_s - \rho_f)\varphi}{V_T(1-\varphi)^m}(u_f - u_s) \right] \mathrm{d}z \tag{17}$$

For simplicity, following Pudasaini (2012), Iverson and Denlinger (2001), Pitman and Le (2005), Pudasaini et al. (2005), Pelanti et al. (2008), the debris flow is assumed to be lithostatic and the constitutive relation can be expressed as

$$\frac{\partial p}{\partial z} = \rho_f g_z \tag{18}$$

$$\frac{\partial}{\partial z}(T_{sxz}) = (\rho_s - \rho_f)\frac{\partial p}{\partial z} \tag{19}$$

The depth-averaged fluid and solid pressures are:

$$p(z_b) = \rho_f g_z h, \quad \overline{p} = \frac{1}{2}\rho_f g_z h, \quad T_{zz}(z_b) = (\rho_f - \rho_s) g_z h, \quad \overline{T}_{szz} = \frac{1}{2}(\rho_s - \rho_f) g_z h$$

The active or passive state of stress is developed if an element of material is elongated or compressed, and the formula for the corresponding states can be derived from the

NHESSD
2, 2151–2183, 2014

Mohrs diagram. It may be easily shown that:

$$k_{\mathrm{ap}} = 2\frac{1 \pm \left[1 - \cos^2\varphi_{\mathrm{int}}\left(1 + \tan^2\varphi_{\mathrm{bed}}\right)\right]^{1/2}}{\cos^2\varphi_{\mathrm{int}}} - 1 \tag{20}$$

In which "–" corresponds to an active state $[\partial u/\partial u\partial x + \partial v/\partial x + \partial v/\partial y \geq 0]_1$ and "+" to be the passive state $[\partial u/\partial u\partial x + \partial v/\partial x + \partial v/\partial y \leq 0]_2$, respectively.

$$\overline{T}_{sxx} = \overline{T}_{sxy} = \frac{1}{2}k_{\mathrm{ap}}(\rho_{\mathrm{s}} - \rho_{\mathrm{f}})g_z h \tag{21}$$

$$\int_{z_{\mathrm{b}}}^{z_{\mathrm{t}}}(\mathrm{RHS})\mathrm{d}z = \rho_{\mathrm{s}}\overline{\varphi}g_x h + \frac{(\rho_{\mathrm{s}} - \rho_{\mathrm{f}})(1-\overline{\varphi})\overline{\varphi}}{V_{\mathrm{T}}(1-\overline{\varphi})^m}(\overline{u}_{\mathrm{f}} - \overline{u}_{\mathrm{s}}) - \frac{\overline{u}_{\mathrm{s}}}{\sqrt{\overline{u}_{\mathrm{s}}^2 + \overline{v}_{\mathrm{s}}^2}}(\rho_{\mathrm{s}} - \rho_{\mathrm{f}})g_z h tg\delta$$
$$- k_{\mathrm{ap}}(\rho_{\mathrm{s}} - \rho_{\mathrm{f}})g_z h\frac{\partial(\overline{\varphi}h)}{\partial x} - \varphi_{\mathrm{b}}(\rho_{\mathrm{s}} - \rho_{\mathrm{f}})g_z h\frac{\partial z_{\mathrm{b}}}{\partial x} + \overline{\varphi}g_z h\frac{\partial(h + z_{\mathrm{b}})}{\partial x}$$

Further, the x momentum conservation equation of the solid phase is expressed as following

$$\frac{\partial\left(h\overline{\varphi}\overline{u}_{\mathrm{s}}\right)}{\partial t} + \frac{\partial\left(h\overline{\varphi}\overline{u}_{\mathrm{s}}^2\right)}{\partial x} + \frac{\partial\left(h\overline{\varphi}\overline{u}_{\mathrm{s}}\overline{v}_{\mathrm{s}}\right)}{\partial y} = \overline{\varphi}g_x h + \frac{(1-\gamma)(1-\overline{\varphi})\overline{\varphi}}{V_{\mathrm{T}}(1-\overline{\varphi})^m}(\overline{u}_{\mathrm{f}} - \overline{u}_{\mathrm{s}}) \tag{22}$$
$$- \frac{\overline{u}_{\mathrm{s}}}{\sqrt{\overline{u}_{\mathrm{s}}^2 + \overline{v}_{\mathrm{s}}^2}}(1-\gamma)g_z h tg\delta - k_{\mathrm{ap}}(1-\gamma)g_z h\frac{\partial(\overline{\varphi}h)}{\partial x} - \varphi_{\mathrm{b}}(1-\gamma)g_z h\frac{\partial z_{\mathrm{b}}}{\partial x} + \overline{\varphi}g_z h\frac{\partial(h + z_{\mathrm{b}})}{\partial x}$$

where $\gamma = \rho_{\mathrm{f}}/\rho_{\mathrm{s}}$.

The depth-integrated equation for the y-momentum component of the solid phase is precisely analogous to those derived above for the x component. Thus, inter-changing

x and y as well as u_s and v_s in the preceding section yield the y-component equations.

$$\frac{\partial\left(h\overline{\varphi}\overline{v}_s\right)}{\partial t}+\frac{\partial\left(h\overline{\varphi}\overline{u}_s\overline{v}_s\right)}{\partial x}+\frac{\partial\left(h\overline{\varphi}\overline{v}_s^2\right)}{\partial y}=\overline{\varphi}g_y h+\frac{(1-\gamma)(1-\overline{\varphi})\overline{\varphi}}{V_T(1-\overline{\varphi})^m}\left(\overline{v}_f-\overline{v}_s\right)\tag{23}$$
$$-\frac{\overline{v}_s}{\sqrt{\overline{u}_s^2+\overline{v}_s^2}}(1-\gamma)g_z h tg\delta-k_{ap}(1-\gamma)g_z h\frac{\partial(\overline{\varphi}h)}{\partial y}-\varphi_b(1-\gamma)g_z h\frac{\partial z_b}{\partial y}+\overline{\varphi}g_z h\frac{\partial(h+z_b)}{\partial y}$$

4.2.2 Fluid-phase

The left-hand side of the x-momentum equation of the fluid phase can be written

$$\mathrm{LHS}=\frac{\partial\rho_f(1-\varphi)u_f}{\partial t}+\frac{\partial\rho_f(1-\varphi)u_f^2}{\partial x}+\frac{\partial\rho_f(1-\varphi)u_f v_f}{\partial y}+\frac{\partial\rho_f(1-\varphi)u_f w_f}{\partial z}$$

Depth averaging and using boundary conditions yields

$$\int_{z_b}^{z_t}\mathrm{LHS}\mathrm{d}z=\int_{z_b}^{z_t}\left[\frac{\partial\rho_f(1-\varphi)u_f}{\partial t}+\frac{\partial\rho_f(1-\varphi)u_f^2}{\partial x}+\frac{\partial\rho_f(1-\varphi)u_f v_f}{\partial y}+\frac{\partial\rho_f(1-\varphi)u_f w_f}{\partial z}\right]\mathrm{d}z$$
$$\int_{z_b}^{z_t}\mathrm{LHS}\mathrm{d}z=\rho_f\left[\frac{\partial(1-\overline{\varphi})h\overline{u}_f}{\partial t}+\frac{\partial(1-\overline{\varphi})h\overline{u}_f^2}{\partial x}+\frac{\partial(1-\overline{\varphi})h\overline{u}_f\overline{v}_f}{\partial y}\right]\tag{24}$$

Depth-averaging the right-hand side of the x-momentum equation of the fluid phase yields:

$$\mathrm{RHS}=\rho_f(1-\varphi)g_x-(1-\varphi)\frac{\partial p}{\partial x}+(1-\varphi)\mu\left[2\frac{\partial}{\partial x}\left(\frac{\partial u_f}{\partial x}\right)+\frac{\partial}{\partial y}\left(\frac{\partial u_f}{\partial y}+\frac{\partial v_f}{\partial x}\right)+\frac{\partial}{\partial z}\left(\frac{\partial u_f}{\partial z}+\right.\right.$$

$$\left.\left.\frac{\partial w_\mathrm{f}}{\partial x}\right)\right] - (1-\varphi)\mu\frac{A}{1-\varphi}\left[2\frac{\partial}{\partial x}\left(\frac{\partial\varphi}{\partial x}(u_\mathrm{f}-u_\mathrm{s})\right) + \frac{\partial}{\partial y}\left(\frac{\partial\varphi}{\partial x}(v_\mathrm{f}-v_\mathrm{s}) + \frac{\partial\varphi}{\partial y}(u_\mathrm{f}-u_\mathrm{s})\right)\right.$$

$$\left.+\frac{\partial}{\partial z}\left(\frac{\partial\varphi}{\partial x}(w_\mathrm{f}-w_\mathrm{s}) + \frac{\partial\varphi}{\partial z}(u_\mathrm{f}-u_\mathrm{s})\right)\right] + (1-\varphi)\frac{(\rho_\mathrm{s}-\rho_\mathrm{f})\varphi}{V_\mathrm{T}(1-\varphi)^m}(u_\mathrm{f}-u_\mathrm{s})$$

$$\int_{z_\mathrm{b}}^{z_\mathrm{t}}(\mathrm{RHS})\mathrm{d}z = \rho_\mathrm{f}(1-\overline{\varphi})g_x h - \frac{(\rho_\mathrm{s}-\rho_\mathrm{f})(1-\overline{\varphi})\overline{\varphi}}{V_\mathrm{T}(1-\overline{\varphi})^m}(\overline{u}_\mathrm{f}-\overline{u}_\mathrm{s}) - (1-\overline{\varphi})\rho_\mathrm{f}g_z h\frac{\partial(h+z_\mathrm{b})}{\partial x}$$

$$+(1-\overline{\varphi})\mu\left[2\frac{\partial^2\overline{u}_\mathrm{f}}{\partial x^2} + \frac{\partial^2\overline{v}_\mathrm{f}}{\partial x\partial y} + \frac{\partial^2\overline{u}_\mathrm{f}}{\partial y^2} - \frac{\chi\overline{u}_\mathrm{f}}{h^2}\right] + \mu A h\left[2\frac{\partial}{\partial x}\left(\frac{\partial\overline{\varphi}}{\partial x}(\overline{u}_\mathrm{f}-\overline{u}_\mathrm{s})\right)\right.$$

$$\left.+\frac{\partial}{\partial y}\left(\frac{\partial\overline{\varphi}}{\partial x}(\overline{v}_\mathrm{f}-\overline{v}_\mathrm{s}) + \frac{\partial\overline{\varphi}}{\partial y}(\overline{u}_\mathrm{f}-\overline{u}_\mathrm{s})\right)\right] - \mu A\frac{\xi\overline{\varphi}(\overline{u}_\mathrm{f}-\overline{u}_\mathrm{s})}{h}$$

where χ is a shape factor that includes vertical shearing of fluid velocity. The shape factor ξ takes into account different distributions of solids volume fraction with depth. For a uniform distribution of velocity in the vertical direction, ξ can be assumed as zero (Pudasaini, 2005).

Further, the x momentum conservation equation of the fluid phase is expressed as following

$$\frac{\partial(1-\overline{\varphi})h\overline{u}_\mathrm{f}}{\partial t} + \frac{\partial(1-\overline{\varphi})h\overline{u}_\mathrm{f}^2}{\partial x} + \frac{\partial(1-\overline{\varphi})h\overline{u}_\mathrm{f}\overline{v}_\mathrm{f}}{\partial y} = (1-\overline{\varphi})g_x h - \frac{(\rho_\mathrm{s}-\rho_\mathrm{f})(1-\overline{\varphi})\overline{\varphi}}{V_\mathrm{T}(1-\overline{\varphi})^m\rho_\mathrm{f}}(\overline{u}_\mathrm{f}-\overline{u}_\mathrm{s})$$

$$-(1-\overline{\varphi})g_z h\frac{\partial(h+z_\mathrm{b})}{\partial x} + \frac{(1-\overline{\varphi})\mu}{\rho_\mathrm{f}}\left[2\frac{\partial^2\overline{u}_\mathrm{f}}{\partial x^2} + \frac{\partial^2\overline{v}_\mathrm{f}}{\partial x\partial y} + \frac{\partial^2\overline{u}_\mathrm{f}}{\partial y^2} - \frac{\chi\overline{u}_\mathrm{f}}{h^2}\right] \quad (25)$$

NHESSD
2, 2151–2183, 2014

A two-phase model for numerical simulation of debris flows

S. He et al.

The depth-integrated equation for the y-momentum component of the fluid phase is precisely analogous to those derived above for the x component.

$$\frac{\partial(1-\overline{\varphi})h\overline{v}_{\mathrm{f}}}{\partial t}+\frac{\partial(1-\overline{\varphi})h\overline{u}_{\mathrm{f}}\overline{v}_{\mathrm{f}}}{\partial x}+\frac{\partial(1-\overline{\varphi})h\overline{v}_{\mathrm{f}}^{2}}{\partial y}=(1-\overline{\varphi})g_y h-\frac{(\rho_{\mathrm{s}}-\rho_{\mathrm{f}})(1-\overline{\varphi})\overline{\varphi}}{V_{\mathrm{T}}(1-\overline{\varphi})^{m}\rho_{\mathrm{f}}}(\overline{v}_{\mathrm{f}}-\overline{v}_{\mathrm{s}})$$
$$-(1-\overline{\varphi})g_z h\frac{\partial(h+z_{\mathrm{b}})}{\partial y}+\frac{(1-\overline{\varphi})\mu}{\rho_{\mathrm{f}}}\left[2\frac{\partial^2\overline{v}_{\mathrm{f}}}{\partial y^2}+\frac{\partial^2\overline{u}_{\mathrm{f}}}{\partial x\partial y}+\frac{\partial^2\overline{v}_{\mathrm{f}}}{\partial x^2}-\frac{\chi\overline{v}_{\mathrm{f}}}{h^2}\right] \tag{26}$$

5 The model equations

The over bars are dropped for brevity. The depth-averaged model equations are written in standard and well structured conservative form. The mass balance equations for the solid and fluid phases are

$$\frac{\partial\varphi h}{\partial t}+\frac{\partial\varphi h u_{\mathrm{s}}}{\partial x}+\frac{\partial\varphi h v_{\mathrm{s}}}{\partial y}=0, \tag{27}$$
$$\frac{\partial(1-\varphi)h}{\partial t}+\frac{\partial(1-\varphi)h u_{\mathrm{f}}}{\partial x}+\frac{\partial(1-\varphi)h v_{\mathrm{f}}}{\partial y}=0, \tag{28}$$

respectively. Similarly, collecting the terms from Eqs. (25) and (29) yields the depth-averaged momentum conservation equations for the solid and the fluid phases

$$\frac{\partial(h\varphi u_{\mathrm{s}})}{\partial t}+\frac{\partial\left(h\varphi u_{\mathrm{s}}^2\right)}{\partial x}+\frac{\partial(h\varphi u_{\mathrm{s}}v_{\mathrm{s}})}{\partial y}=\varphi g_x h+\frac{(1-\gamma)(1-\varphi)\varphi}{V_{\mathrm{T}}(1-\varphi)^{m}}(u_{\mathrm{f}}-u_{\mathrm{s}}) \tag{29}$$
$$-\frac{u_{\mathrm{s}}}{\sqrt{u_{\mathrm{s}}^2+v_{\mathrm{s}}^2}}(1-\gamma)g_z h tg\delta-k_{\mathrm{ap}}(1-\gamma)g_z h\frac{\partial(\varphi h)}{\partial x}-\varphi_{\mathrm{b}}(1-\gamma)g_z h\frac{\partial z_{\mathrm{b}}}{\partial x}+\varphi g_z h\frac{\partial(h+z_{\mathrm{b}})}{\partial x}$$

$$\frac{\partial(h\varphi v_s)}{\partial t} + \frac{\partial(h\varphi u_s v_s)}{\partial x} + \frac{\partial\left(h\varphi v_s^2\right)}{\partial y} = \varphi g_y h + \frac{(1-\gamma)(1-\varphi)\varphi}{V_T(1-\varphi)^m}(v_f - v_s)$$
$$- \frac{v_s}{\sqrt{u_s^2+v_s^2}}(1-\gamma)g_z h tg\delta - k_{ap}(1-\gamma)g_z h\frac{\partial(\varphi h)}{\partial y} - \varphi_b(1-\gamma)g_z h\frac{\partial z_b}{\partial y} + \varphi g_z h\frac{\partial(h+z_b)}{\partial y} \tag{30}$$

$$\frac{\partial(1-\varphi)hu_f}{\partial t} + \frac{\partial(1-\varphi)hu_f^2}{\partial x} + \frac{\partial(1-\varphi)hu_f v_f}{\partial y} = (1-\varphi)g_x h - \frac{(\rho_s-\rho_f)(1-\varphi)\varphi}{V_T(1-\varphi)^m\rho_f}(u_f - u_s)$$
$$-(1-\varphi)g_z h\frac{\partial(h+z_b)}{\partial x} + \frac{(1-\varphi)\mu}{\rho_f}\left[2\frac{\partial^2 u_f}{\partial x^2} + \frac{\partial^2 v_f}{\partial x\partial y} + \frac{\partial^2 u_f}{\partial y^2} - \frac{\chi u_f}{h^2}\right] \tag{31}$$

$$\frac{\partial(1-\varphi)hv_f}{\partial t} + \frac{\partial(1-\varphi)hu_f v_f}{\partial x} + \frac{\partial(1-\varphi)hv_f^2}{\partial y} = (1-\varphi)g_y h - \frac{(\rho_s-\rho_f)(1-\varphi)\varphi}{V_T(1-\varphi)^m\rho_f}(v_f - v_s)$$
$$-(1-\varphi)g_z h\frac{\partial(h+z_b)}{\partial y} + \frac{(1-\varphi)\mu}{\rho_f}\left[2\frac{\partial^2 v_f}{\partial y^2} + \frac{\partial^2 u_f}{\partial x\partial y} + \frac{\partial^2 v_f}{\partial x^2} - \frac{\chi v_f}{h^2}\right] \tag{32}$$

Equations (26)–(31) allow the debris flow depth h, volume fraction of the solid φ, and the depth-averaged velocity components for solid u_s and v_s, and for fluid u_f and v_f to be computed as functions of space and time, once appropriate initial and (numerical) boundary conditions are prescribed.

6 Discussion

In this paper, based on the shallow water assumption and depth-average integration, a system of model equations of two-phase debris flow is constituted. The model employs the Mohr–Coulomb plasticity for the solid stress, and the fluid stress is modeled as a Newtonian viscous stress. The relative motion and interaction between the solid

NHESSD
2, 2151–2183, 2014

and fluid phases are also considered. The system equations differ from the conservation equations used in many previous models of two-phase as summarized in Table 1.

The fluid phase of debris flows can deviate from an ideal fluid, depending on the constituents forming the fluid phase, which can include silt, clay, and fine particles. In natural debris flows, viscosity can range from 0.001 to 10 Pa s or higher. A small change in the fluid viscosity may lead to substantial change in the dynamics of the debris flow motion (Pudasaini, 2012). Therefore, Pitman and Le model and Bouchut model in which the fluid phase are considered as ideal fluid are not reasonable, and more suitable for dilute debris flow. Iverson mixture models are only quasi two-phase or virtually single-phase because they neglect differences between the fluid and solid velocities. Thus, drag force cannot be generated, more suitable for dense debris flow. Pudasaini model (2012) is a relatively perfect two-phase flow model, the model takes into account the effect of buoyancy, drag force and virtual mass But the model is too complex and not easy to apply. The present model which considers the interaction between solid phase and liquid phase, including buoyancy, drag force, employing the Mohr–Coulomb plasticity for the solid stress, and the fluid stress is modeled as a Newtonian viscous stress. The present model is relatively simple and is advantageous for the numerical solution and application

7 Model verification

To further assess the capability of the model proposed to reproduce debris flow phenomena, comparisons between the present model and Pitman and Le model have been made. For comparison, only the one-dimensional computational case of debris flow motion is considered. In one-dimensional case, the equations are further reduced to

$$\left.\begin{array}{l}
\frac{\partial \varphi h}{\partial t}+\frac{\partial \varphi h u_{\mathrm{s}}}{\partial x}=0 \\
\frac{\partial(1-\varphi) h}{\partial t}+\frac{\partial(1-\varphi) h u_{\mathrm{f}}}{\partial x}=0 \\
\frac{\partial(h \varphi u_{\mathrm{s}})}{\partial t}+\frac{\partial\left(h \varphi u_{\mathrm{s}}^2+\frac{1}{2} k_{\mathrm{ap}} g_z(1-r) \varphi h^2\right)}{\partial x}+\frac{1}{2} r g_z \varphi \frac{\partial h^2}{\partial x}= \\
g_x \varphi h+\frac{(1-\gamma)(1-\varphi) \varphi h}{V_{\mathrm{T}}(1-\varphi)^m}(u_{\mathrm{f}}-u_{\mathrm{s}})-r g_z \varphi h \frac{\partial b}{\partial x}-k_{\mathrm{ap}}(1-\gamma) g_z \varphi h \frac{\partial b}{\partial x} \\
-\operatorname{sgn}(u_{\mathrm{s}}) \varphi h g_z(1-r) \tan \theta_{\mathrm{bed}} \\
\frac{\partial(1-\varphi) h u_{\mathrm{f}}}{\partial t}+\frac{\partial(1-\varphi) h u_{\mathrm{f}}^2}{\partial x}+\frac{1}{2}(1-\varphi) g_z \frac{\partial h^2}{\partial x}= \\
g_x(1-\varphi) h-\frac{(1-\gamma)(1-\varphi) \varphi h}{V_{\mathrm{T}}(1-\varphi)^m}(u_{\mathrm{f}}-u_{\mathrm{s}})-g_z(1-\varphi) h \frac{\partial b}{\partial x} \\
+\frac{(1-\varphi) \mu}{\rho_{\mathrm{f}}}\left(2 \frac{\partial^2 u_{\mathrm{f}}}{\partial x^2}-\frac{\chi u_{\mathrm{f}}}{h^2}\right)
\end{array}\right\} \tag{33}$$

7.1 Formulation in h_{s}, h_{f}

We now rewrite our model by expressing quantities containing the variables φ and h in terms of the conserved quantities $h_{\mathrm{s}}=\varphi h$ and $h_{\mathrm{f}}=(1-\varphi) h$. Manipulating suitably the Eq. (33), we obtain the system

$$\left.\begin{array}{l}
\frac{\partial h_{\mathrm{s}}}{\partial t}+\frac{\partial h_{\mathrm{s}} u_{\mathrm{s}}}{\partial x}=0 \\
\frac{\partial h_{\mathrm{f}}}{\partial t}+\frac{\partial h_{\mathrm{f}} u_{\mathrm{f}}}{\partial x}=0 \\
\frac{\partial(h_{\mathrm{s}} u_{\mathrm{s}})}{\partial t}+\frac{\partial\left(h_{\mathrm{s}} u_{\mathrm{s}}^2+\frac{1}{2} g_z h_{\mathrm{s}}^2\left(k_{\mathrm{ap}}(1-\gamma)+\gamma\right)+\frac{1}{2} k_{\mathrm{ap}} g_z(1-\gamma) h_{\mathrm{s}} h_{\mathrm{f}}\right)}{\partial x}+\gamma g_z h_{\mathrm{s}} \frac{\partial h_{\mathrm{f}}}{\partial x} \\
=g_x h_{\mathrm{s}}+\frac{(1-\gamma)(1-\varphi) \varphi(h_{\mathrm{s}}+h_{\mathrm{f}})}{V_{\mathrm{T}}(1-\varphi)^m}(u_{\mathrm{f}}-u_{\mathrm{s}})-\left[k_{\mathrm{ap}}(1-\gamma) g_z h_{\mathrm{s}}+\gamma g_z h_{\mathrm{s}}\right] \frac{\partial b}{\partial x} \\
-\operatorname{sgn}(u_{\mathrm{s}}) h_{\mathrm{s}} g_z(1-r) \tan \theta_{\mathrm{bed}} \\
\frac{\partial h_{\mathrm{f}} u_{\mathrm{f}}}{\partial t}+\frac{\partial\left(h_{\mathrm{f}} u_{\mathrm{f}}^2+\frac{1}{2} g_z h_{\mathrm{f}}^2\right)}{\partial x}+g_z h_{\mathrm{f}} \frac{\partial h_{\mathrm{s}}}{\partial x} \\
=g_x h_{\mathrm{f}}-\frac{(1-\gamma)(1-\varphi) \varphi h}{V_{\mathrm{T}}(1-\varphi)^m}(u_{\mathrm{f}}-u_{\mathrm{s}})-h_{\mathrm{f}} g_z \frac{\partial b}{\partial x}+\frac{(1-\varphi) \mu}{\rho_{\mathrm{f}}}\left(2 \frac{\partial^2 u_{\mathrm{f}}}{\partial x^2}-\frac{\chi u_{\mathrm{f}}}{(h_{\mathrm{s}}+h_{\mathrm{f}})^2}\right)
\end{array}\right\} \tag{34}$$

NHESSD

2, 2151–2183, 2014

A two-phase model for numerical simulation of debris flows

S. He et al.

where θ is the angle of inclination of the bed slope as shown in Fig. 2.

The calculated flows are shown schematically in Fig. 2. It was assumed that a fluid-solid mixture was initially contained on the slope by a vertical wall to form a semicircular pile (diameter 3.0 m) as indicated in Fig. 2 at time $t = 0$. The debris flow was released from rest on the rough incline and the flow velocities and surge shapes were determined at later times $t > 0$. The bed inclination angle $\theta = 30^\circ$. The solids bed friction angle $\delta = 25^\circ$ and the internal friction angle was chosen as $\varphi_{\text{int}} = 35^\circ$. The density of solid phase and the fluid phase are 2400 kN m^{-3} and 1150 kN m^{-3}, respectively. The volume fraction of the solid phase $\varphi = 0.7$. The viscosity of the fluid phase $\mu = 0.001$ Pa s.

Equation (34) can be recast in vector conservation form as

$$\frac{\partial \boldsymbol{U}}{\partial t} + \frac{\partial \boldsymbol{F}}{\partial x} = \boldsymbol{S} \tag{35}$$

with vectors $\boldsymbol{U}$, $\boldsymbol{F}$ and $\boldsymbol{S}$ defined as follows

$$\boldsymbol{U} = \begin{pmatrix} h_s \\ h_s u_s \\ h_f \\ h_f u_f \end{pmatrix}, \quad \boldsymbol{F} = \begin{pmatrix} h_s u_s \\ h_s u_s^2 + \frac{1}{2} g_z h_s^2 (k_{ap}(1-\gamma) + \gamma) + \frac{1}{2} k_{ap} g_z (1-\gamma) h_s h_f \\ h_f u_f \\ h_f u_f^2 + \frac{1}{2} g_z h_f^2 \end{pmatrix}, \tag{36}$$

$$\boldsymbol{S} = \begin{pmatrix} 0 \\ \left(\begin{array}{c} g_x h_s + \frac{(1-\gamma)(1-\varphi)\varphi(h_s+h_f)}{V_T(1-\varphi)^m}(u_f - u_s) - [k_{ap}(1-\gamma) g_z h_s + \gamma g_z h_s] \frac{\partial b}{\partial x} \\ -\gamma g_z h_s \frac{\partial h_f}{\partial x} - \mathrm{sgn}(u_s) h_s g_z (1-r) \tan\theta_{\text{bed}} \end{array} \right) \\ 0 \\ g_x h_f - \frac{(1-\gamma)(1-\varphi)\varphi h}{V_T(1-\varphi)^m}(u_f - u_s) - g_z h_f \frac{\partial h_s}{\partial x} - h_f g_z \frac{\partial b}{\partial x} + \frac{(1-\varphi)\mu}{\rho_f}\left(2\frac{\partial^2 u_f}{\partial x^2} - \frac{\chi u_f}{(h_s+h_f)^2}\right) \end{pmatrix} \tag{37}$$

7.2 Eigenspace

The governing Eq. (35) can be written in non-conservation form as

$$\frac{\partial \boldsymbol{U}}{\partial t} + \mathbf{A}\frac{\partial \boldsymbol{U}}{\partial x} = \boldsymbol{S} \tag{38}$$

with the Jacobian matrix **A** defined as

$$\mathbf{A} = \begin{bmatrix} 0 & 1 & 0 & 0 \\ c_s^2 - u_s^2 & 2u_s & c_s' h_s & 0 \\ 0 & 0 & 0 & 1 \\ 0 & 0 & c_f^2 - u_f^2 & 2u_f \end{bmatrix} \tag{39}$$

where u_s and h_f denote the depth-averaged velocity for each layer, and where the sign c_s, c_f and c_f' are defined as follows:

$$\left.\begin{array}{l} c_s^2 = k_{ap} g_z (1-\gamma) h_s + g_z h_s + \frac{1}{2} k_{ap} g_z (1-r) h_f \\ c_f^2 = g_z h_f \\ c_s' = \frac{1}{2} k_{ap} g_z (1-r) \end{array}\right\} \tag{40}$$

The eigenvalues of **A** are real and distinct

$$\left.\begin{array}{l} \lambda_s^{(1)} = u_s - c_s \\ \lambda_s^{(2)} = u_s + c_s \\ \lambda_f^{(1)} = u_f - c_f \\ \lambda_f^{(2)} = u_f + c_f \end{array}\right\} \tag{41}$$

It is noted that Note that c_s' does not bear any physical meaning such as a wave propagation speed in still fluid and it is introduced for the convenience of notation only.

NHESSD
2, 2151–2183, 2014

A two-phase model for numerical simulation of debris flows

S. He et al.

Assuming that we can accurately calculate the eigenspeeds λ_p, we can then find the eigenvectors by solving

$$\begin{bmatrix} 0 & 1 & 0 & 0 \\ c_s^2 - u_s^2 & 2u_s & c'_s h_s & 0 \\ 0 & 0 & 0 & 1 \\ 0 & 0 & c_f^2 - u_f^2 & 2u_f \end{bmatrix} \cdot \begin{bmatrix} 1 \\ \alpha_1 \\ \alpha_2 \\ \alpha_3 \end{bmatrix} = \begin{bmatrix} \lambda_p \\ \alpha_1\lambda_p \\ \alpha_2\lambda_p \\ \alpha_3\lambda_p \end{bmatrix} \tag{42}$$

These equations imply that $\alpha_1 = \lambda_p$ and $\alpha_3 = \lambda_p\alpha_2$. We then have two equations for one unknown α_2 which should satisfy the second and fourth equations simultaneously. Solving this two equations and we have

$$\alpha_{2,\mathrm{p}} = \begin{cases} \frac{(\lambda_p - u_s)^2 - c_s^2}{c'_s h_s}, & \text{and} \\ \frac{c_f^2}{(\lambda_p - u_f)^2 - c_f^2} \end{cases} \tag{43}$$

where the subscript of p corresponds to the appropriate eigenvalue. We can use either form of α_2 in Eq. (43) and obtain the final form of the eigenvectors as $[1, \lambda_p, \alpha_p, \alpha_p\lambda_p]^{\mathrm{T}}$.

7.3 Solving method

In this paper, we use fractional step method to solve the problem and the 1-D Riemann problem at the cell interface is solved using Roe's approximation. The computational procedure are expressed as follows.

Step 1: Solving the homogeneous SWE

$$\frac{\partial \boldsymbol{U}}{\partial t} + \mathbf{A}\frac{\partial \boldsymbol{U}}{\partial x} = 0 \tag{44}$$

The Roe's approximation is used for the linearized system Eq. (44) and the final expression of Roe's format is

$$U'_i = U_i^n + \frac{\mathrm{d}t}{\mathrm{d}x}(F_{i-\frac{1}{2}} - F_{i+\frac{1}{2}}) \tag{45}$$

NHESSD
2, 2151–2183, 2014

where $\mathrm{d}t$ is time step and $\mathrm{d}x$ is grid length, $F_{i+\frac{1}{2}} = \frac{1}{2}(F_i + F_{i+1}) - \frac{1}{2}\sum_{j=1}^{2} \alpha_p \left|\lambda_p\right| \kappa_p$ and κ_p can be obtained by solving

$$\Delta \boldsymbol{U} \equiv \begin{pmatrix} \Delta U_1 \\ \Delta U_2 \\ \Delta U_3 \\ \Delta U_4 \end{pmatrix} = \sum_{p=1}^{4} \alpha_p \kappa_p \tag{46}$$

Step 2: Solve the source term

$$\frac{\partial \boldsymbol{U}}{\partial t} = \boldsymbol{S} \tag{47}$$

To reduce numerical instabilities, a semi-implicit method is used and the equation is discretized as below:

$$\frac{U_i^{n+1} - U_i'}{\Delta t} = S_i' \tag{48}$$

where U_i' and S_i' are the solutions of Step 1.

7.4 Numerical experiment

In order to verify the model accuracy, we calculate a dam-break problem at first according to the parameters of Pitman (2005). The initial conditions consist of two constant states separated by interface located at $x = 5$. We define the initial values of the flow height and the solid volume fraction as

$$\begin{aligned} &h = 3, \quad \varphi = 0.7, \quad u_\mathrm{s} = -1.4, \quad u_\mathrm{f} = 0.3 \quad \text{if } x < 5 \quad \text{and} \\ &h = 2, \quad \varphi = 0.4, \quad u_\mathrm{s} = -0.9, \quad u_\mathrm{f} = 0.1 \quad \text{if } x > 5 \end{aligned} \tag{49}$$

NHESSD
2, 2151–2183, 2014

The computational results are displayed in Fig. 3.

As we know that it may produce spurious oscillations if the numerical schemes are not well-balanced in numerical tests. The computation result of dam-break problem using our model agrees well with the result of Pitman (2005). Through the test of dam-break problem it indicates that our numerical method is able to capture the physically correct reflected waves.

After the model feasibility experiment, a case of debris flow is computed using our model. The initial condition of the debris flow is configured as shown in Fig. 2. In Fig. 4 we display the spatial and temporal evolution of a two-phase debris flow as the mixture moves down an inclined channel as shown in the insert for $t = 3, 6, 10\,\mathrm{s}$, it is observed that the height of debris changes from high to low and gradually accumulates with the bed inclination angle decrease. The collapse and accumulation of debris flow can also be found in Fig. 4. At the same time, the velocity of debris flow at different time is shown in Fig. 5. Here, the overall velocity $u = \frac{\rho_s \varphi u_s + \rho_f (1-\varphi) u_f}{\rho}$ and $\rho = \rho_s \varphi + (1-\varphi)\rho_f$. It is shown that the solid phase and the liquid phase is separated gradually during activity. The solid phase is focus on the front of debris flow and corresponding to this is an increase of the volume fraction. This is a commonly observed phenomena in granular-rich debris flows, in which the front is solids-rich and the main body is followed by a fluid-rich tail (Iverson, 1997; Iverson and Denlinger, 2001; Pudasaini et al., 2005). The mass flows moving down an incline can be divided into three sections. The bed inclination angle of upper parts of the incline ($0 \le x \le 120$) is $\theta = 30^\circ$, the bed inclination angle of middle part ($120 < x \le 200$) is decrease progressively and the third section ($200 < x \le 400$) is horizontal. The initial height of debris flow is 4 m and the extent 40 m. The boundary conditions are zero because we set the computational domain is sufficiently large.

An important aspect of the two-phase debris flow simulation is the solid volume fraction. The size of it has great influences the movement of debris flow. In this paper, we also compare the movement of debris flow with different volume fraction (Fig. 6). Initially the height of debris flow $h = 4\,\mathrm{m}$, the solid volume fraction is $\varphi = 0.3$ and $\varphi = 0.9$,

Discussion Paper | Discussion Paper | Discussion Paper | Discussion Paper |

NHESSD

2, 2151–2183, 2014

the conditions of the other are same. Three times has been used to represent the movement of debris as $t = 3$, 7, 10 s. Here, we should notice the viscous parameter μ, it is a commonly observed phenomena that the viscous of debris flow is get higher with the increasing of the volume fraction, so when we use different volume fraction to simulation the movement of debris, the viscous parameter μ should be different. Following debris collapse, the debris with lower solid volume fraction is moving faster and the distance of two debris flow is greater. Note that, the debris with low volume fraction is easier to disperse so its tail is longer. This is the liquid phase character reflect in the process of movement of debris flow.

Another important aspect of the two-phase debris flow simulation is the fluid viscosity. In Pitman model (2005), the fluid is considered as inviscid fluid and thus the effects of fluid viscosity on the movement has been ignored. In order to reflect the important of fluid viscosity in the process of debris flow, we compare our model with Pitman model (2005) (Fig. 7). Initially the height of debris flow $h = 4$ m, the volume fraction of debris $\varphi = 0.7$ and other conditions is same as Fig. 2. Three times has been used to represent the movement of debris as $t = 3$, 6, 9 s. In this simulation, it is observed that the movement of debris flow is slower if the fluid viscosity is considered. Because of considering fluid viscosity, the resistance in debris flow increases so that the velocity of debris decreases correspondingly. It is noted that the debris considering fluid viscosity has a longer tail, It shows that the friction force between debris and ground increases because of fluid viscosity. Therefore, the importance of fluid viscosity in the process of movement of debris flow cannot be ignored.

8 Conclusion

In the paper, a novel two-phase model of debris flow has been presented. The model is based on a two-phase formulation and it has been derived from mass and momentum conservation principles applied to debris flow based on the shallow water assumption and depth-average integration. Mohr–Coulomb plasticity is used to close the solid stress. The fluid stress is modeled as a Newtonian viscous stress. The system equations differ from the conservation equations used in many previous models of two-phase. Firstly, a dam-break problem is calculated to indicate that our model can describe the complex dynamics of two-phase debris flows. On the other hand, in order to display the importance of fluid viscosity in the process of movement of debris flow, several numerical experiments have been presented. The Pitman and Le's model ignores the viscosity influence of fluid phase may overestimate the mobility of two-phase debris flow. We compare our model with Pitman model (2005) and prove that the fluid viscosity is an undeniable role in debris flow movement. Base on the importance of fluid viscosity, we consider the effect of different volume fraction in the process of movement of debris flow, debris flow shape has been presented at different times. Simulation results demonstrate that viscous stress of fluid phase and volume fraction of solid phase significantly affects the flow dynamics. The results of this model hint that an entrainment model can lead to a better practice in the quantification of hazards.

Acknowledgements. We acknowledge the financial support from the National Key Basic Research Program of China (2013CB733201), NSFC (Grant No. 41272346, 41101008), and the Key Research Program of the Chinese Academy of Sciences (KZZD-EW-05-01).

References

Anderson, K., Sundaresan, S., and Jackson, R.: Instabilities and the formation of bubbles in fluidized beds, J. Fluid Mech., 303, 327–336, 1995.

Bouchut F., Fernandez-Niet E. D., Mangeney A., and Narbona-Reina G.: A two-phase shallow debris flow model with energy balance, 21 March, 2013.

Cao, Z., Pender, G., Wallis, S., and Carling, P.: Computational dam-break hydraulics over erodible sediment bed, J. Hydraul. Eng., 130, 689–703, 2004.

Capart, H. and Young, D.: Formation of a jump by the dam-break wave over a granular bed, J. Fluid Mech., 372, 165–187, 1998.

Denlinger, R. P. and O'Connell, D. R. H.: Simulations of cataclysmic outburst floods from Pleistocene Glacial Lake Missoula, Geol. Soc. Am. Bull., 122, 678–689, 2010.

George, D. L. and LeVeque R. J.: Finite volume methods and adaptive refinement for global tsunami propagation and local inundation, 2006.
Gray, J. M. N. T., Wieland, M., and Hutter, K.: Gravity-driven free surface flow of granular avalanches over complex basal topography, P. R. Soc. A, 455, 1841–1874, 1999.
Hungr, O.: A model for the run-out analysis of rapid flow slides, debris flows, and avalanches, Can. Geotech. J., 32, 610–623, 1995.
Hutter, K. and Koch, T.: Motion of a granular avalanche in an exponentially curved chute: experiments and theoretical predictions, Philos. T. R. Soc. A, 334, 93–138, 1991.
Hutter, K., Svendsen, B., and Rickenmann, D.: Debris flow modelling: a review, Continuum Mech. Therm., 8, 1–35, 1996.
Iverson, R. M.: The physics of debris flows, Rev. Geophys., 35, 245–296, 1997.
Iverson, R. M.: Elementary theory of bed–sediment entrainment by debris flows and avalanches, J. Geophys. Res., 117, F03006, doi:10.1029/2011JF002189, 2012.
Iverson, R. M. and Denlinger, R. P.: Flow of variably fluidized granular masses across three dimensional terrain, 1. Coulomb mixture theory, J. Geophys. Res., 106, 537–552, 2001.
Iverson, R. M., Logan, M., LaHusen, R. G., and Berti, M.: The perfect debris flow? Aggregated results from 28 large-scale experiments, J. Geophys. Res., 115, F03005, doi:10.1029/2009JF001514, 2010.
Jackson, R.: The Dynamics of Fluidized Particles, Cambridge University Press, Cambridge, 2000.
McDougall, S. and Hungr, O.: Dynamic modelling of entrainment in rapid landslides, Can. Geotech. J., 42, 1437–1448, 2005.
Medina, V., Hürlimann, M., and Bateman, A.: Application of FLATModel, a 2D finite volume code, to debris flows in the northeastern part of the Iberian Peninsula, Landslides, 5, 127–142, 2008.
Pelanti, M., Bouchut, F., and Mangeney, A.: A roe-type scheme for two-phase shallow granular flows over variable topography, ESAIM:M2AN, 42, 851–885, 2008.
Pitman, E. B. and Le, L.: A two-fluid model for avalanche and debris flows, Philos. T. R. Soc. A, 363, 1573–1602, 2005.
Pitman, E., Nichita, C., Patra, A., Bauer, A., Bursik, M., and Weber, A.: A model of granular flows over an erodible surface, Discrete Cont. Dyn.-B, 3, 589–600, 2003.
Pudasaini, S. P.: Some exact solutions for debris and avalanche flows, Phys. Fluids, 23, 043301, doi:10.1063/1.3570532, 2011.

Pudasaini, S. P.: A general two-phase debris flow model, J. Geophys. Res., 117, F03010, doi:10.1029/2011JF002186, 2012.
Pudasaini, S. P. and Hutter, K.: Rapid shear flows of dry granular masses down curved and twisted channels, J. Fluid Mech., 495, 193–208, 2003.
Pudasaini, S. P., Wang, Y., and Hutter, K.: Modelling debris flows down general channels, Nat. Hazards Earth Syst. Sci., 5, 799–819, doi:10.5194/nhess-5-799-2005, 2005.
Richardson, J. F. and Zaki, W. N.: Sedimentation and fluidization: part I., Trans. Inst. Chem. Eng., 32, 35–53, 1954.
Rickenmann, D.: Empirical relationships for debris flows, Nat. Hazards, 19, 47–77, 1999.
Savage, S. B. and Hutter, K.: The motion of a finite mass of granular material down a rough incline, J. Fluid Mech., 199, 177–215, 1989.
Soares-Frazão, S., Canelas, R., Cao, Z., Cea, L., Chaudhry, H. M., Die Moran, A., El Kadi, K., Ferreira, R., Fraga Cadórniga, I., Gonzalez-Ramirez, N., Greco, M., Huang, W., Imran, J., Le Coz, J., Marsooli, R., Paquier, A., Pender, G., Pontillo, M., Puertas, J., Spinewine, B., Swartenbroekx, C., Tsubaki, R., Villaret, C., Wu, W., Yue, Z., and Zech, Y.: Dam-break flows over mobile beds: experiments and benchmark tests for numerical models, J. Hydraul. Res., 50, 364–375, 2012.
Tai, Y. C., Noelle, S., Gray, J. M. N. T., and Hutter, K.: Shock-capturing and front-tacking methods for dry granular avalanches, J. Comput. Phys., 175, 269–301, 2002.

Table 1. Comparisons of other author's two-phase model of debris flow with present model.

Authors	Theoretical principle	Solid phase	Fluid phase	Interaction forces
Iverson (1997) Iverson and Denlinger (2001)	Coulomb mixture theory	Savage–Hutter model	Newtonian fluids $\tau_{ij} = -\left(p + \frac{2}{3}\mu\nabla\cdot\boldsymbol{u}\right)\delta_{ij} + 2\mu e_{ij}$	–
Pitman and Le (2005)	phase-averaged theory	Savage–Hutter model	Ideal fluid $\tau_{ij} = p\delta_{ij}$	$f = (1-\varphi)\beta(\boldsymbol{u}-\boldsymbol{v})$ $\beta = \frac{(\rho^{s}-\rho^{f})\varphi\boldsymbol{g}}{V_t(1-\varphi)^m}$
Pudasaini (2012)	phase-averaged theory	Savage–Hutter model	Non-Newtonian fluid $\boldsymbol{\tau}_f = \eta_f\left[\nabla\cdot\boldsymbol{u}_f + (\nabla\cdot\boldsymbol{u}_f)^t\right] - \eta_f\frac{A(\alpha_f)}{\alpha_f}\left[(\nabla\cdot\alpha_s)(\boldsymbol{u}_f-\boldsymbol{u}_s) + (\boldsymbol{u}_f-\boldsymbol{u}_s)(\nabla\cdot\alpha_s)\right]$	$M_s = C_{DG}(u_f-u_s)\lvert u_f-u_s\rvert$ $-C_{VMG}\frac{d}{dt}(u_f-u_s)$
Bouchut (2013)	dissipative energy balance	Savage–Hutter model	Ideal fluid $\tau_{ij} = p\delta_{ij}$	$f = (1-\varphi)\beta(\boldsymbol{u}-\boldsymbol{v})$ $\beta = \frac{(\rho^{s}-\rho^{f})\varphi\boldsymbol{g}}{V_T(1-\varphi)^m}$
Present model (2013)	phase-averaged theory	Savage–Hutter model	Newtonian fluid $\tau_{ij} = -\left(p + \frac{2}{3}\mu\nabla\cdot\boldsymbol{u}\right)\delta_{ij} + 2\mu e_{ij}$	$f = (1-\varphi)\beta(\boldsymbol{u}-\boldsymbol{v})$ $\beta = \frac{(\rho^{s}-\rho^{f})\varphi\boldsymbol{g}}{V_T(1-\varphi)^m}$

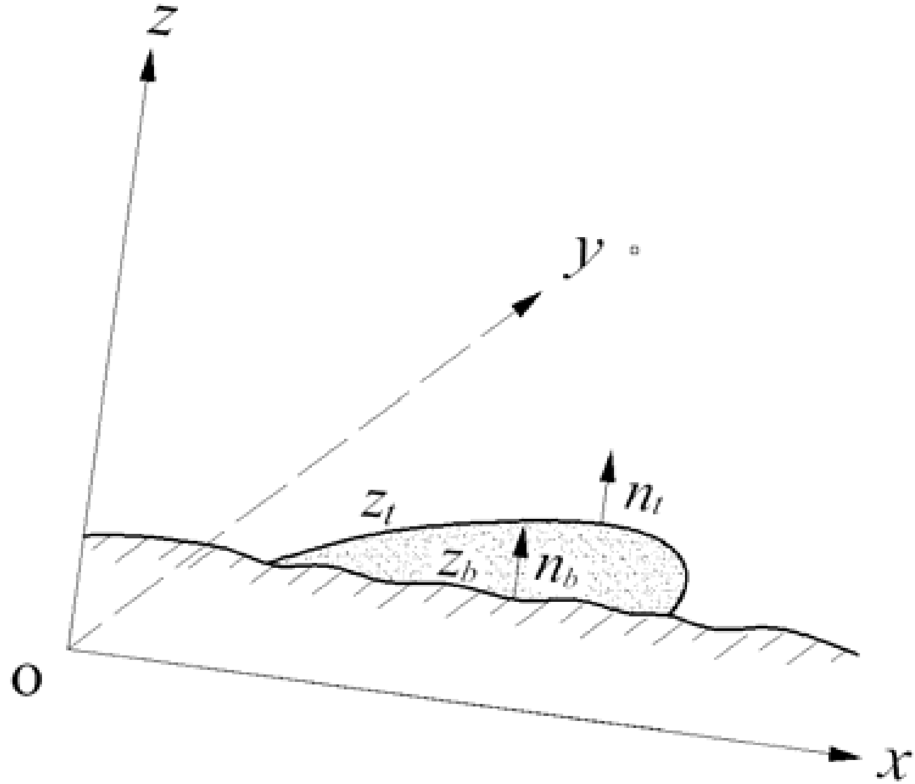

Fig. 1. Schematic diagram of the coordinate system and boundary of debris flow.

NHESSD
2, 2151–2183, 2014

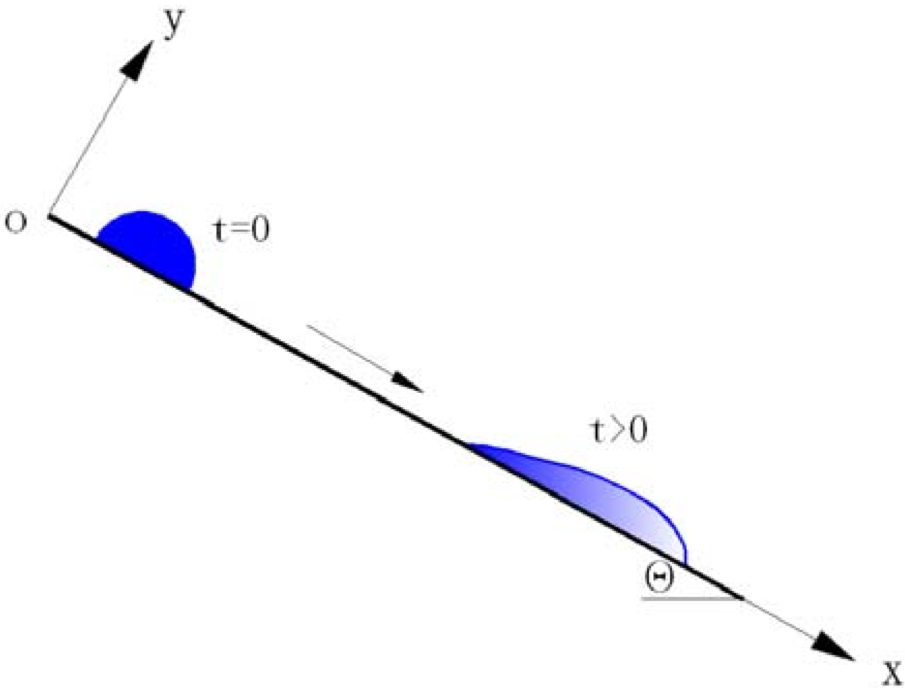

Fig. 2. Schematic diagram of the release of a finite mass of debris flow on a rough incline.

NHESSD
2, 2151–2183, 2014

A two-phase model for numerical simulation of debris flows

S. He et al.

Title Page
Abstract Introduction
Conclusions References
Tables Figures
◀I ▶I
◀ ▶
Back Close
Full Screen / Esc
Printer-friendly Version
Interactive Discussion

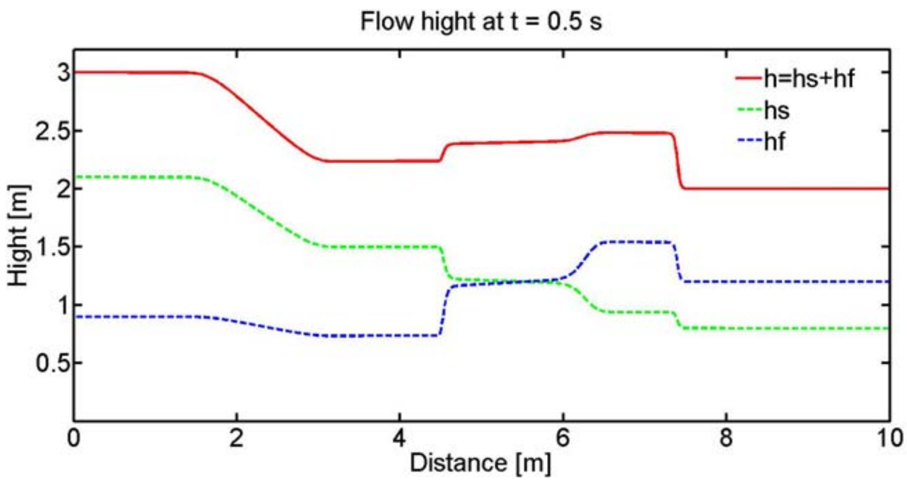

Fig. 3. Compuational results of flow depth h (red line), variables h_s (green line) and h_f (blue line) at $t = 0.5$ s. The computational result of dam-break problem using our model accords with the result of Pitman (2005). It is proved that our model is able to capture the physically correct reflected waves.

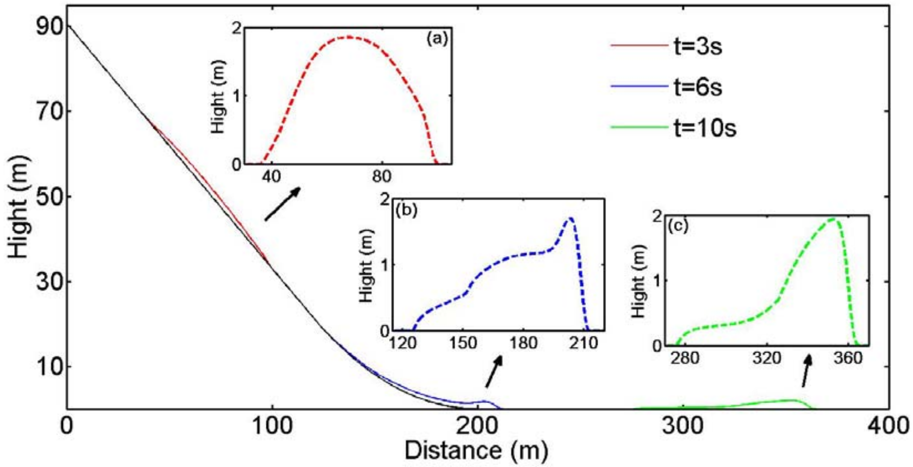

Fig. 4. Spatial and temporal evolution of a two-phase debris flow as the mixture moves down an inclined channel is shown in the insert at $t = 3$, 6, 10 s. Initially, the height of debris flow $h = 4$ m, the volume fraction $\varphi = 0.7$. The evolution of the debris flow, at different time, represent by different color solid line, respectively. **(a–c)** are the partial enlarged view of debris flow at different time, represent by the dash line correspond to the same color solid line. It is observed that the height of debris is change from high to low and gradually accumulation with the bed inclination angle decrease.

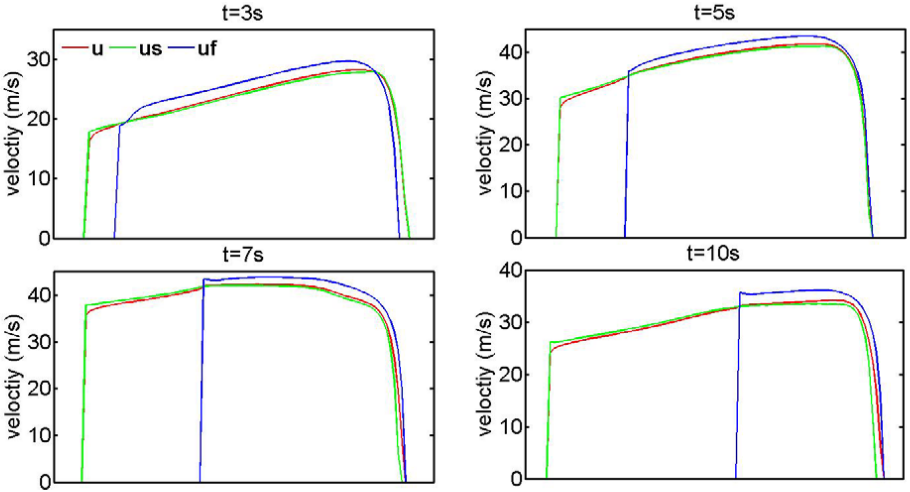

Fig. 5. The figure shows the spatial and temporal evolution of velocity of a two-phase debris flow with different time of $t = 3, 5, 7, 10\,\mathrm{s}$. The initial condition of Fig. 5 is same as Fig. 4. The overall velocity, solid phase velocity and liquid phase velocity is represented by different color solid line. Note that, in the process of debris flow movement, the range of velocity of solid phase is focus on the front of debris flow gradually; it is show that the solid phase and liquid phase is separately. Corresponding to the change of the solid phase velocity, the front volume fraction of debris flow is increased and the back volume fraction is decrease.

NHESSD
2, 2151–2183, 2014

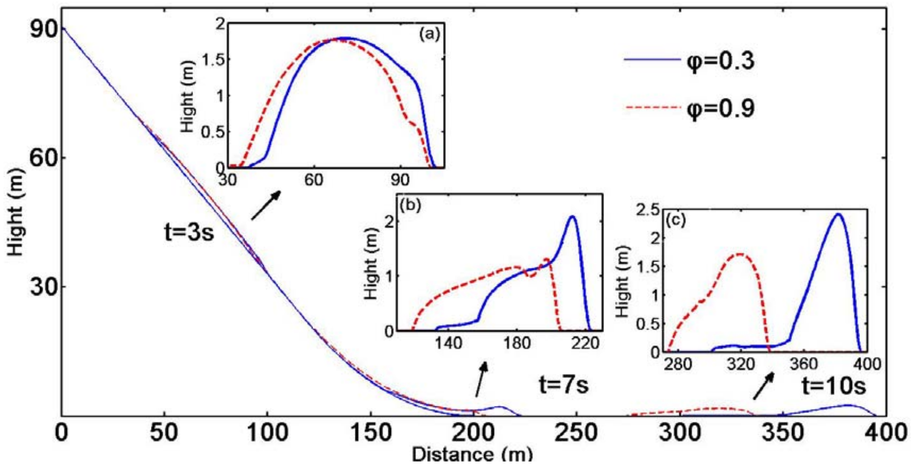

Fig. 6. In the figure the movement of debris with different volume fraction is shown, three times as $t = 3$, 7, 10 s has been used to plot the shape of debris flow. The debris with $\varphi = 0.3$ is represent by solid line and the dash line is $\varphi = 0.9$. **(a–c)** are the partial enlarged view of debris flow at different time. It is observed that the debris flow is move slow down with the higher of volume fraction so that the distance of two debris flow is greater and also it is easier to pile up. Note that, the tail of debris with low volume fraction is longer than anther. This is the liquid phase character reflect in the process of movement of debris flow.

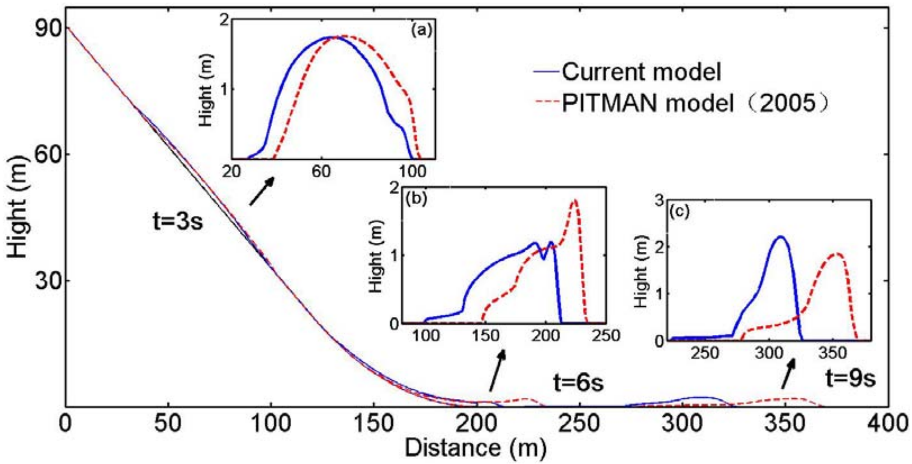

Fig. 7. We set that the parameter between two models is same. The volume fraction $\varphi = 0.7$ and we plot the movement of the debris flow at different time as t = 3, 6, 9 s. **(a–c)** is the partial enlarged view of debris flow at different time. It is easy to find that the movement of debris flow is slower if the fluid viscosity is considered. Because of consideration of fluid viscosity, the resistance in debris flow is increase so that the velocity of debris is decrease corresponding. Note that, the debris consider fluid viscosity has a longer tail, It shows that the friction force between debris and ground is increase because of fluid viscosity. So the importance of fluid viscosity in the process of movement of debris flow cannot be ignored.

NHESSD
2, 2151–2183, 2014